

FSW of aluminum AA5754 to steel DX54 with innovative overlap joint

Gonçalo Sorger¹ · Hao Wang¹ · Pedro Vilaça¹  · Telmo G. Santos²

Received: 7 September 2016 / Accepted: 9 December 2016 / Published online: 4 January 2017
© The Author(s) 2017. This article is published with open access at Springerlink.com

Abstract An innovative overlap joint concept was tested to evaluate the quality improvement of welds between aluminum alloy AA5754-H22 (2 mm) and steel DX54 (1.5 mm). The innovation is a wave-shaped interface produced on the steel being directly processed by the tip of the probe, generating localized heat, extensive chemically active surfaces, and additional mechanical interlocking. Welds with different parameters were evaluated by metallographic analysis and mechanical tests. The best set of parameters was then implemented in a conventional overlap joint, plus in two- and three-passes welding, with the innovative overlap joint concept, to evaluate the effect on microstructure and mechanical efficiency. With a single-pass weld, the new concept presented lower strength in tensile shear tests, but higher strength in peeling tests. The main mechanism governing this behavior was the reduction of effective thickness in the aluminum alloy sheet, due to the flow of steel into the aluminum alloy. The characterization and distribution of the intermetallic compounds were evaluated via SEM-EDX. The two-passes weld resulted in the best strength values in tensile shear tests, reaching about 50% of the ultimate tensile strength of the aluminum alloy base material.

Keywords (IIW Thesaurus) Friction stir welding · Dissimilar materials · Al Mg alloys · Steels · Intermetallics · Mechanical tests

1 Introduction

Energy saving and minimizing environmental impact are important challenges for automotive industries. One efficient solution for these challenges is to use car body structures sharing lightweight and corrosion resistance aluminum alloy (AA) in conjunction with tough steel. The main difficulty in the manufacturing of car body structures with dissimilar materials is the joining of these two materials, mainly due to the differences in physical and chemical properties as stated by Kenevisi and Khoie [1]. Mechanical joining methods, such as clinching, riveting, and bolt joining, are well established in many car manufacturing companies for joining dissimilar materials [2, 3]. Nonetheless, the interlocking effectiveness of these mechanical joining methods is limited by either materials anisotropy or stress concentration at the joining zone. According to Abe et al. [4], the high strength of steels results in the deformation of fasteners when piercing the overlapped materials and the stress concentration leads to the distortion of joints, thereby decreasing the interlocking effectiveness. Compared to these mechanical joining methods, welding allows a continuous joint between the materials. Fusion welding methods, such as laser welding and gas tungsten arc welding (GTAW), operate above the melting point of the base materials. Dehghani et al. [5] mentioned that the high heat input can create a large amount of brittle intermetallic compounds (IMCs) in the weld zone, which is detrimental to the mechanical resistance of the welds. To reduce the formation of IMCs, solid-state welding methods such as ultrasonic welding and friction stir welding (FSW) can be employed because of their low heat input [6]. In order to obtain a more reliable AA to steel joint for automotive

Recommended for publication by Commission III - Resistance Welding, Solid State Welding, and Allied Joining Process

✉ Pedro Vilaça
pedro.vilaca@aalto.fi

¹ Department of Mechanical Engineering, School of Engineering, Aalto University, Espoo, Finland

² UNIDEMI, Departamento de Engenharia Mecânica e Industrial, Faculdade de Ciências e Tecnologia, Universidade Nova de Lisboa, 2829-516 Caparica, Portugal

applications, an innovative friction stir overlap joint concept was developed and tested in this investigation.

Leitão et al. [7] studied AA5000 and AA6000 series, which are very popular in automotive industry for car skin sheet applications. Extensive research has been done on welding steel, such as SS400 [8] and St52 [5], to AA5083 [8], AA5186 [5], AA5754 [9], AA6013 [10], AA6061 [11–13], and AA6181 [11]. These steels have relatively low yield strength but excellent formability, making them well suited for vehicle inner panel applications. The thickness of the investigated plates ranged from 2 to 4 mm. Little research was reported on very thin plates, less than 2 mm thick [13, 14].

Some authors tested conventional FSW of AA to steel. Liu et al. [12] studied the effects of process parameters on the microstructure evolution in joints of butt welded 1.5 mm AA6061-T651 to TRIP780/800 steel. The results show that the joint exhibited 85% of the ultimate tensile strength of the AA with the fracture occurring in the heat-affected zone (HAZ) of the AA. The reason suggested for the location of the fracture in the HAZ is due to the overaging with dissolution of the fine precipitates within the AA due to the extra heat transfer from the mechanical processing of the steel surface. Coelho et al. [11] reported the characterization of the microstructure formation of 1.5 mm AA6181-T4 and HC340LA steel sheet by FSW of overlap joints. Their research showed that the maximum force obtained in shear tests reached 73% of the AA6181-T4 base material. Fracture occurred on the retreating side of the AA6181-T4 stir zone where steel fragments were present. To improve weld quality, some authors proposed modifications of the conventional FSW method. Sur Bang et al. [13] utilized hybrid friction stir welding (HFSW) assisted with GTAW to butt weld 3-mm-thick AA6061-T6 AA and STS304

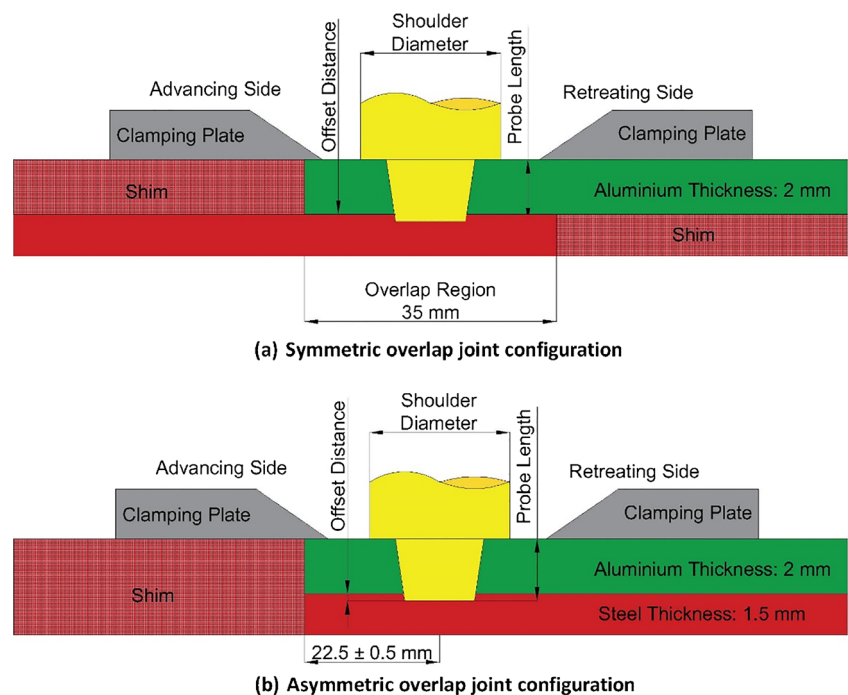
stainless steel. The GTAW was used for preheating the stainless steel, which increased material flow of the steel, resulting in improved mechanical resistance. The maximum tensile strength of the HFSW joint reported was 93% of the AA base metal. Similarly, Liu et al. [14] employed electrically assisted FSW for butt welding 1.4-mm-thick AA6061 to TRIP780 steel. Two electrodes were positioned close to the FSW tool, on the steel side. The steel softened via the electro-plastic effect, which led to enhanced formation of thin layers of IMC. The synergic effect of both the electro-plastic effect and Joule heating can help reduce axial welding force and facilitate the initial plunge stage.

The aim of the present work is to evaluate a new overlap joint concept for dissimilar FSW of typical automotive sheet metal aluminum alloy AA5754-H22 to steel DX54. The innovation is a wave-shaped interface produced on the steel being directly processed by the tip of the probe, generating localized heat, extensive chemically active surfaces in a layered structure, and additional mechanical interlocking. The effect on microstructure and mechanical efficiency of the process parameters was investigated for single pass welding. For comparison, the best set of parameters were implemented in a conventional overlap joint and two- and three-pass welds with the new joint concept.

2 Joint design

In the present investigation, two FSW overlap joint configurations (symmetric and asymmetric) were tested for welding AA to steel with conventional and innovative concepts. Figure 1 depicts the symmetric and asymmetric overlap joint configurations. Unlike the planar interfaces of conventional

Fig. 1 Geometrical arrangement and details on the symmetric (for tensile shear test) and asymmetric (for peeling test) overlap joint configurations



overlap joint configurations, the weld interface in the innovative overlap joint configurations have a wave-shaped geometry embossed in the steel side, as shown in Fig. 2. This feature was produced on the steel sheet using a roller, with the negative profile of the wave feature, over a planar anvil with the steel sheet in the middle. During the welding, the probe will process the central and lateral vertices of the wave-like feature, resulting in localized intense plastic deformation and heat generation. This action results in chemically active surfaces promoting localized solid-state joining mechanisms via interfacial diffusion and atomic bonding. When traveling, the probe pushes the AA into the concavities of the wave-shaped feature contributing to a mechanical locking effect.

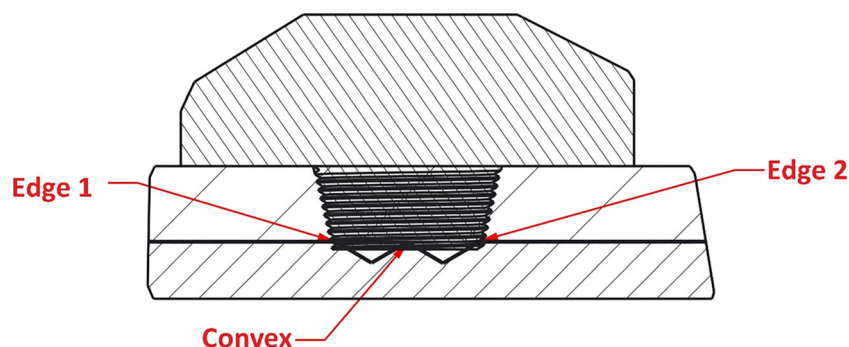
3 Experimental plan

The experimental plan to evaluate the innovative FSW overlap joint design is established in Table 1. In the first step, three sets of parameters were tested, for both the symmetrical and asymmetrical innovative overlap joint configurations. Specimens for optical microscopic observation, tensile shear tests, and peeling tests were extracted. For each mechanical test, four specimens were tested for each condition. The set of parameters that produced the joint with the best mechanical properties were then used in the next steps, namely in step 2 with conventional overlap joint, and step 3 with the multipass innovative overlap joint. Peeling tests were not carried out in step 3. Step 4 was further investigation of the single-pass welds, implemented with the best set of parameters from step 1; they underwent microhardness testing and scanning electron microscopy (SEM) examination with energy-dispersive X-ray (EDX) analysis.

4 Experimental conditions

The AA5754-H22 and DX54 steel were used as base materials for all experiments. The sheets of both metals had a length of 300 mm and a width of 150 mm. The thickness of the AA sheets was 2 mm, whereas that of the steel sheets was 1.5 mm. The welding direction was always along the rolling direction

Fig. 2 Representation of the “innovative overlap joint” design configuration with the wave-shaped geometry embossed in the steel side semi-processed by the tip of the probe of the FSW tool



of the base materials, which corresponds to the direction along the length of the sheets. The chemical compositions and mechanical properties of the base materials are presented in Tables 2 and 3, respectively.

The modular FSW tool is composed of a smooth shoulder, conical probe, and tool body, as shown in Fig. 3. The shoulder diameter was 17 mm, with 3.6° concavity. The length of the probe was 2.7 mm. The largest diameter of the conical probe was 5 mm, and the smallest diameter of the probe was 4 mm. Moreover, the conical probe has left-handed threaded with 1.5-mm pitch and 1-mm depth. The left-handed (LH) orientation of the threads was used with a clockwise rotation direction to generate a vertical flow of the AA towards the steel. Both the shoulder and the probe were made from H13 steel, as in previous studies from other authors [5, 15]. The main welding parameters for the single-pass welding of the innovative overlap joint (step 1) are shown in Table 4.


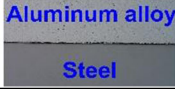


5 Analysis of results

5.1 Analysis of step 1

Optical macrographs of the three different weld parameters for the innovative symmetric overlap joint are shown in Fig. 4. The left column shows the locations and features of voids. A large void was found in weld 1, and a number of smaller voids are found in the steel stir zone of weld 3. These voids can reduce the strength of the welds. In comparison, weld 2 has the smallest voids. The right column shows the macrographs of these welds after chemical etching. The yellow circles highlight the interlocking regions. The most relevant mechanical interlocking feature is formed in Weld 3.

The optical micrographs in position 1 and position 2 show that layered structures exist in the steel stir zone of weld 2 and weld 3. These structures are the mixture of AA and steel, which facilitate the atomic bonding of the overlapped materials. Authors Coelho et al. [10] mentioned that these layered structures can also provide an additional bonding mechanism, thereby increasing the strength of the welds. The axial forging force during weld 1 was smaller than for other the welds,

Table 1 Experimental plan

Step 1	Innovative overlap joint (single pass)			
	Weld 1	Optical Microscopic Analysis	Tensile Shear Test ↔	Peeling Test ↗ ↘
	Weld 2			
	Weld 3			
Establishment of the best set of parameters for further analysis in the following steps: Best (Weld i) _{$i=1, \dots, 3$} \equiv FSW _{new}				
Step 2	Conventional overlap joint (single pass) with the best set of parameters found in Step 1: FSW _{conv}			
	Optical Microscopic Analysis	Tensile Shear Test ↔	Peeling Test ↗ ↘	
Step 3	Innovative Overlap Joint (multi-pass): FSW _{new} with 2 passes ; FSW _{new} with 3 passes			
	2 Passes	Optical Microscopic Analysis	Tensile Shear Test ↔	
	3 Passes			
Step 4	Further analysis of innovative overlap joint (single pass)			
	Microhardness Test		SEM + EDX Analysis	

which may explain why no distinct layered structure was observed.

Swirl-like patterns, visible in weld 1 and weld 2, are not formed in weld 3. These patterns are the outcome of the thermomechanical history and disappear when travel speed is increased. According to Kimapong et al. [16] and Elrefaey et al. [17], the decreased of the travel speed results in increased heat input. Excessive heat input could have accelerated the formation of IMCs in weld 1, which is detrimental to its mechanical resistance.

Cantin et al. [18] described that a threaded probe led to the formation of a steel hook within the AA. The hook size can affect the mechanical strength of the joint by causing a reduction in the effective thickness of the AA sheet. Figure 5 shows the effective thickness of the AA sheets at the flow side, i.e., the retreating side for the welds. Weld 2 presents the lowest reduction in effective thickness due to the hook formation effect. Weld 1 has 1.29 mm and weld 3 has only 0.9 mm of

Table 2 Chemical composition (wt.%) of the base materials

AA5754-H22	Mg	Si	Fe	Cu	Mn	Cr	Zn	Ti	Al
	2.6–3.6	0.4	0.4	0.1	0.5	0.3	0.2	0.15	Remaining
DX54	C	Si	Mn	P		S		Ti	Fe
	0.12	0.5	0.6	0.1		0.045		0.3	Remaining

Table 3 Mechanical properties of the base materials

Material	Yield strength (MPa)	Ultimate tensile strength (MPa)	Elongation (%)	Hardness (HV02)
AA5754-H22	192	257	14.8	68
DX54	165	287	52.4	107

Fig. 3 The friction stir welding tool: **a** shoulder (smooth with 3.6° concavity and 17-mm diameter); **b** probe (conical with LH threads of 1.5-mm pitch); **c** shoulder and probe assembled in tool body



Table 4 The main welding parameters for the single pass welding of the innovative overlap joint

Identification	Travel speed (mm/min)	Axial force (kN)	Rotation speed (rpm)	Initial plunge depth of probe (mm)
Weld 1	100	3.5	800	2.7
Weld 2	200	7.5		
Weld 3	400	12		

effective thickness, both of which are thinner than in weld 2 with 1.44 mm.

Figure 6a shows the results of the tensile shear test for the innovative joint in symmetric overlap configuration. Weld 2 exhibits the best tensile shear strength at 177 N/mm, which is

35% of the UTS of the unwelded AA sheet. Weld 3 exhibits a tensile shear strength of 169 N/mm. The failure load of weld 1 is 124 N/mm, the worst result, only 25% of the UTS of the AA sheet. Furthermore, two distinct fracture modes were identified, as shown in Fig. 6b. In the tensile shear test, all the specimens from weld 1, and half the specimens from weld 3, fractured through the weld interface (mode 1). The mode 1 failure is presumably due to the voids present in the stir zone of the steel, which is consistent with previous microstructure observations. Alternatively, all specimens from weld 2 and half from weld 3 fractured at the AA base material (mode 2).

The force-displacement curves of the innovative asymmetric overlap joints, which display the history of the peeling strength, are shown in Fig. 7. Weld 1 exhibits the worst results, with a maximum load of 453 N. In agreement with the microstructure analysis, insufficient axial forging force, absence of the layered structured and excessive heat input (leading to

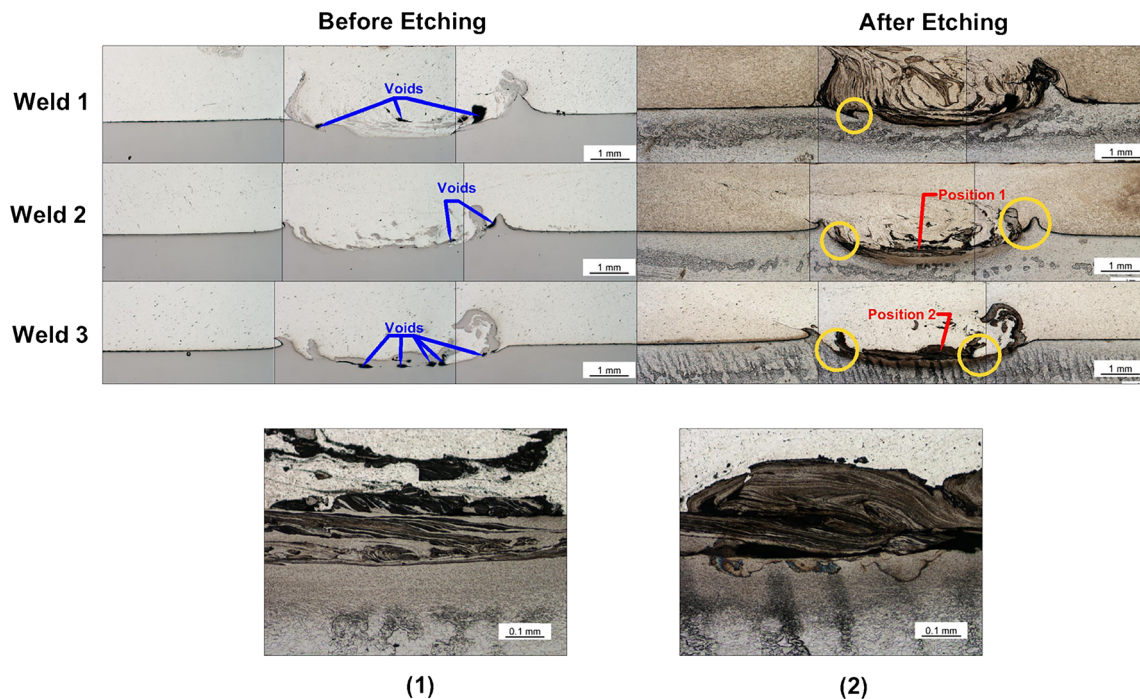


Fig. 4 Optical macrographs of weld 1, weld 2, and weld 3. Also included are the optical micrographs emphasizing the layered structure from position 1 and position 2 of the “after etching” condition

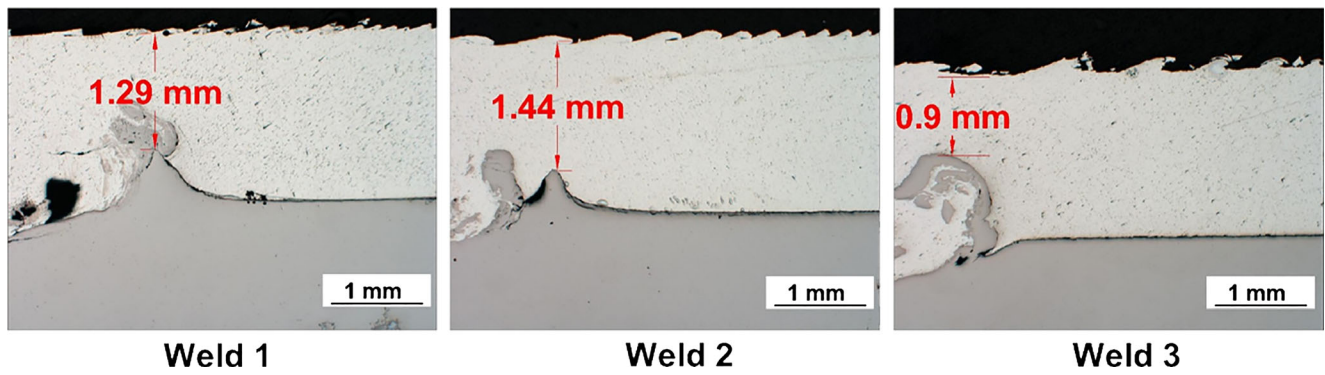
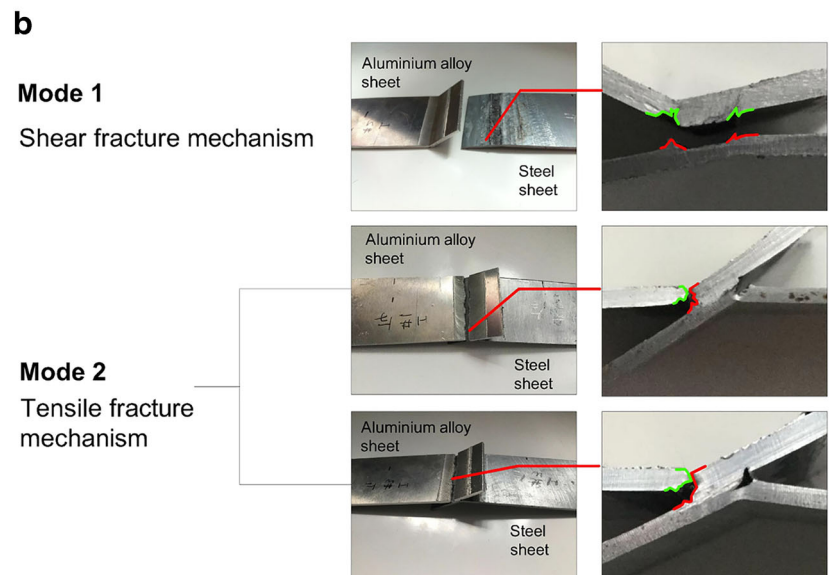
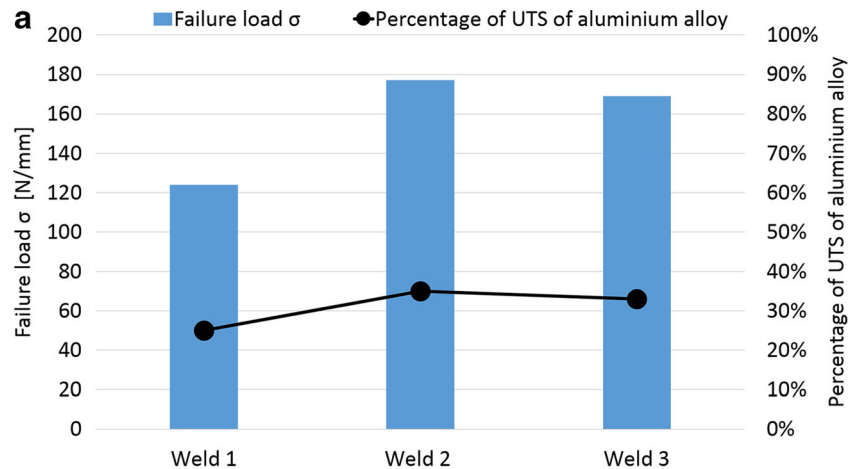


Fig. 5 The effective thickness of aluminum alloy (AA) of weld 1, weld 2, and weld 3

thicker IMCs along the weld interface) should be the reasons why weld 1 had the lowest strength. In addition, the force-displacement curve for weld 1 exhibits a step-shape variation after reaching maximum load, which is consistent with the presence of voids on the weld interface, as seen in Fig. 4. The maximum peeling test loads of weld 2 and weld 3 were

1150 and 1000 N, respectively. Out of the three welds, weld 2 achieved the highest displacement while the value for weld 1 was the lowest. Welds 2 and 3 did not exhibit the step-shape behavior since the final fracture happened at the AA sheet, similar to the failure mode in the tensile shear test. The bonding strength of weld 2 and weld 3 drops gradually after

Fig. 6 Results of the tensile shear test of the innovative overlap joints. **a** Failure load; **b** the two main modes of fracture: mode 1—shear fracture, and mode 2—tensile fracture with the crack initiating from the hook. For mode 2, a distinct fracture path may exist



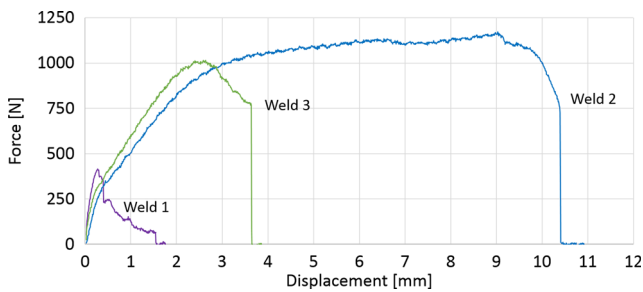


Fig. 7 Force-displacement curves for peeling test of the innovative overlap joints: weld 1, weld 2, and weld 3

reaching the maximum loads, due to the crack propagation along the hooks, until ultimately breaking at the thin residual cross section of the AA sheet. The interlocking features of weld 2 and weld 3 could have also provided additional mechanical bonding strength. Overall, weld 2 has the best performance; thus, its welding parameters were selected for further testing in the next steps and will hereafter be referred to as FSW_{new}.

5.2 Analysis of step 2

In step 2, the performance of the welds with the best set of parameters for the innovative overlap joint design (FSW_{new}) were compared with a conventional overlap joint configuration, also in single pass with the same parameters. These samples, named as FSW_{conv}, were then tested and the results were compared to those obtained for FSW_{new}. Figure 8 shows the

optical macrographs of these two overlap joint configurations. Compared to the innovative overlap joint (FSW_{new}), the conventional overlap joint (FSW_{conv}) has more, and larger, voids which have a detrimental influence on its mechanical resistance.

At the middle of the weld bead, a swirl-like material flow pattern was observed in FSW_{new}; however, this pattern has not been detected in FSW_{conv}. This fact maybe due to the extra heat generated during the direct processing by the tip of the probe on the convex part of the wave-shaped geometry embossed in the steel, for the FSW_{new} condition. This resulted in a condition more prone to the formation of the swirl-like material flow pattern.

Figure 9 shows the effective thickness of the AA sheets of these two welds. Considering the effect of the hook on the effective thickness, it is possible to conclude that in the innovative overlap joint the residual thickness is slightly lower than that of the conventional overlap joint. Figures 8 and 9 show some larger Fe rich particles at the retreating side of FSW_{conv}, which are detrimental for the joint strength.

Figure 10a shows the tensile shear and peeling test results. FSW_{new} exhibits lower tensile shear strength, 177 N/mm, which is 35% of the UTS of the AA base material. FSW_{conv} exhibits higher tensile shear strength of 203 N/mm, which is 40% of the UTS of the AA base material. The fracture of both welds occurred in the AA sheet (mode 2), likely due to the reduction of the effective thickness caused by the hooks. The small difference between the effective thicknesses of the AA sheet of FSW_{new} versus FSW_{conv} may explain the difference

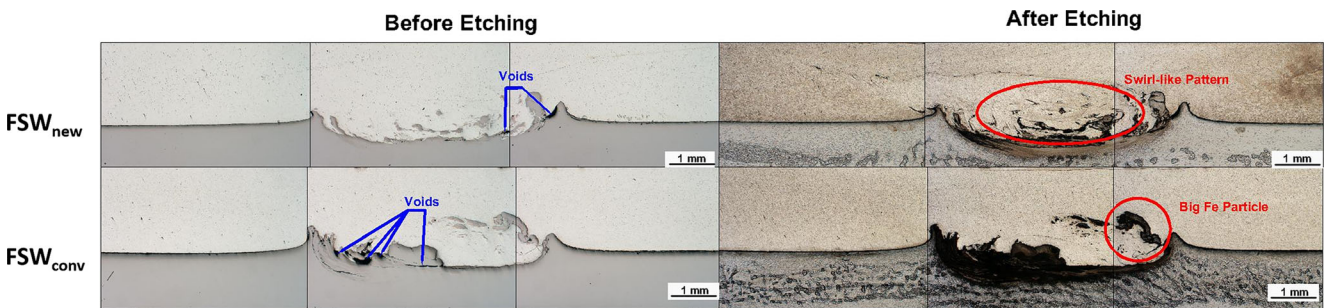
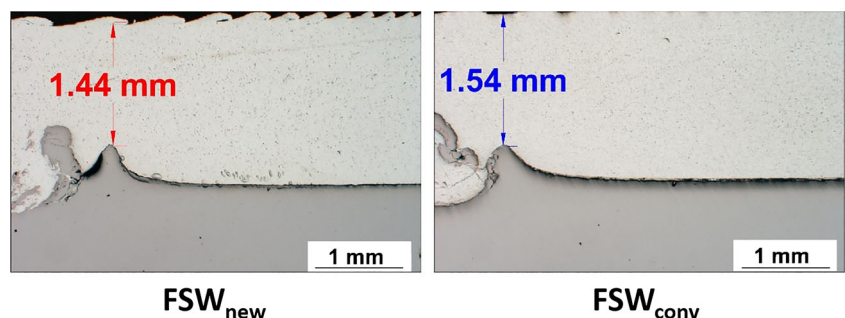


Fig. 8 Optical microscopic analysis comparing between the macrostructure of the innovative overlap joint (FSW_{new}) and the conventional overlap joint (FSW_{conv}) produced with same technological conditions as FSW_{new}

Fig. 9 The effective thickness of the AA of the best innovative overlap joint (FSW_{new}) and the conventional overlap joint (FSW_{conv}) produced with same technological conditions as FSW_{new}



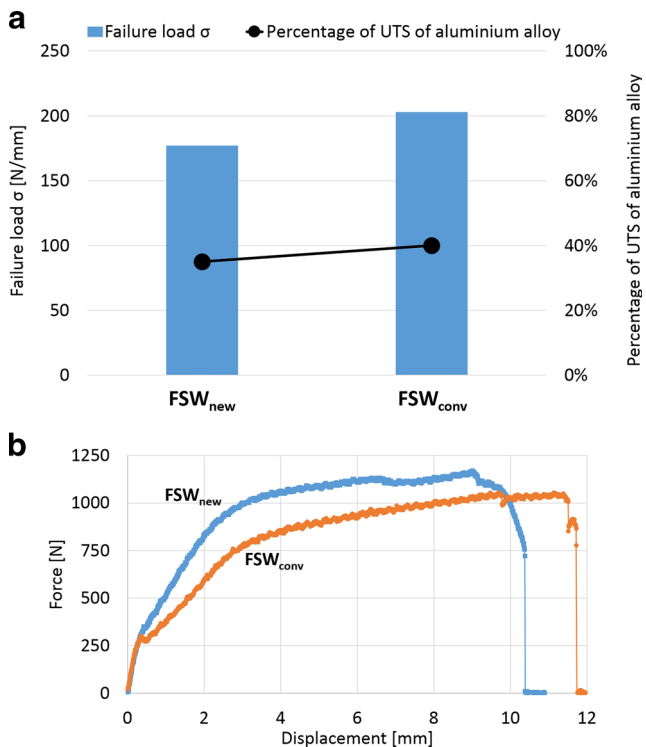


Fig. 10 Comparative test results of FSW_{new} and FSW_{conv}: **a** tensile shear test results with fracture initiated from the hook (mode 2); **b** history of the results for the peeling tests

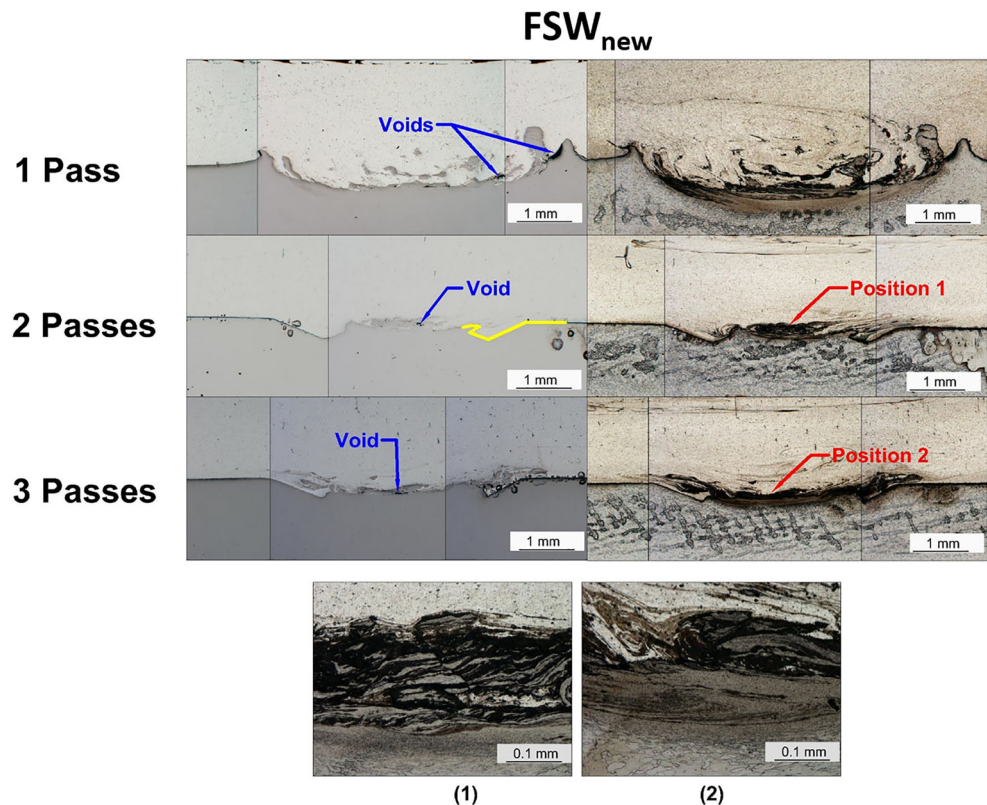
in the maximum tensile shear strength between these two welds.

Figure 10b presents the force-displacement history of the force along the joint opening in the peeling test. Both welding conditions exhibit a long propagation period under the maximum load plateau. At the limit conditions, the fractures occurred in the AA base material. In contrast with the tensile shear test results, the maximum strength during the peeling test of FSW_{new} is higher than that of FSW_{conv}. This may be due to the presence of larger Fe particles at the retreating side of FSW_{conv}. The large Fe particles act as imperfections, resulting in the reduction of the effective thickness of the AA base material.

5.3 Analysis of step 3

Figure 11 shows the optical macrographs of the single and multipass FSW_{new} welds. The multipass welds exhibit fewer voids. This can be attributed to higher stirring efficiency, which improves material flow within the processing zone, eliminating the voids. The multipass welds also present fewer mixture layers since they produce more heat and, therefore, a greater amount of steel is stirred and distributed into the processing zone of the AA sheet. On the bottom of Fig. 11, micrographs of positions 1 and 2 show details of the mixture layers. The yellow curve highlights a hook-shaped interlocking feature that is present in the weld with two passes.

Fig. 11 Optical microscopic analysis comparing the single-pass weld with the multipass welds (two passes and three passes) for the innovative overlap joint, where the multipass welds were implemented with the same welding parameters as FSW_{new}. Also included, micrographs emphasizing the accumulated Fe particles in position 1 (two passes) and position 2 (three passes)



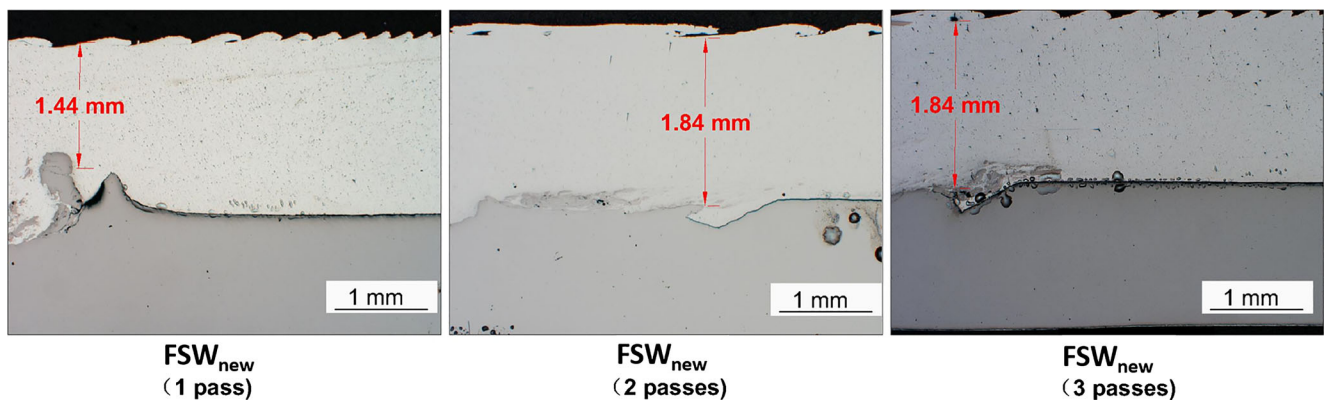


Fig. 12 The effective thickness of the AA of FSW_{new} with one-pass, two-pass, and three-pass welding procedure

However, such a feature is not observed on the weld with three passes since the rotating probe destroyed it during the third pass. As can be seen in Fig. 12, the effective thickness of the innovative overlap joint is the same for both of the multipass welds and is higher overall than in the single-pass welding procedure.

The results of the tensile shear tests are shown in Fig. 13. FSW_{new} with single-pass welding has 177 N/mm tensile shear strength, which is 35% of the UTS of AA base material. FSW_{new} with two passes has 252 N/mm shear strength, which is 50% of the UTS of AA base material. FSW_{new} with three passes has 188 N/mm, which is 37% of the UTS of AA base material. The fracture in FSW_{new} with single pass welding occurred at the AA sheet (mode 2). However, the fractures in the multipass welds were located at the weld interface (mode 1). According to previous microstructure observation, some Fe particles accumulated on the weld interface of both multipass welds, which may have contributed to the reduction in joint strength. Emphasis should be given to the fact that the innovative overlap joint welded with two passes exhibits the highest strength value from all the mechanical test trials. As per prior microstructure observation from Fig. 11, an additional interlocking feature formed in the grooves of this joint, which might have provided the additional mechanical joining that led to a higher mechanical resistance.

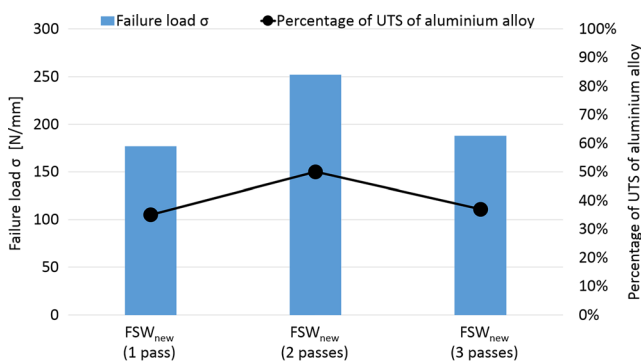


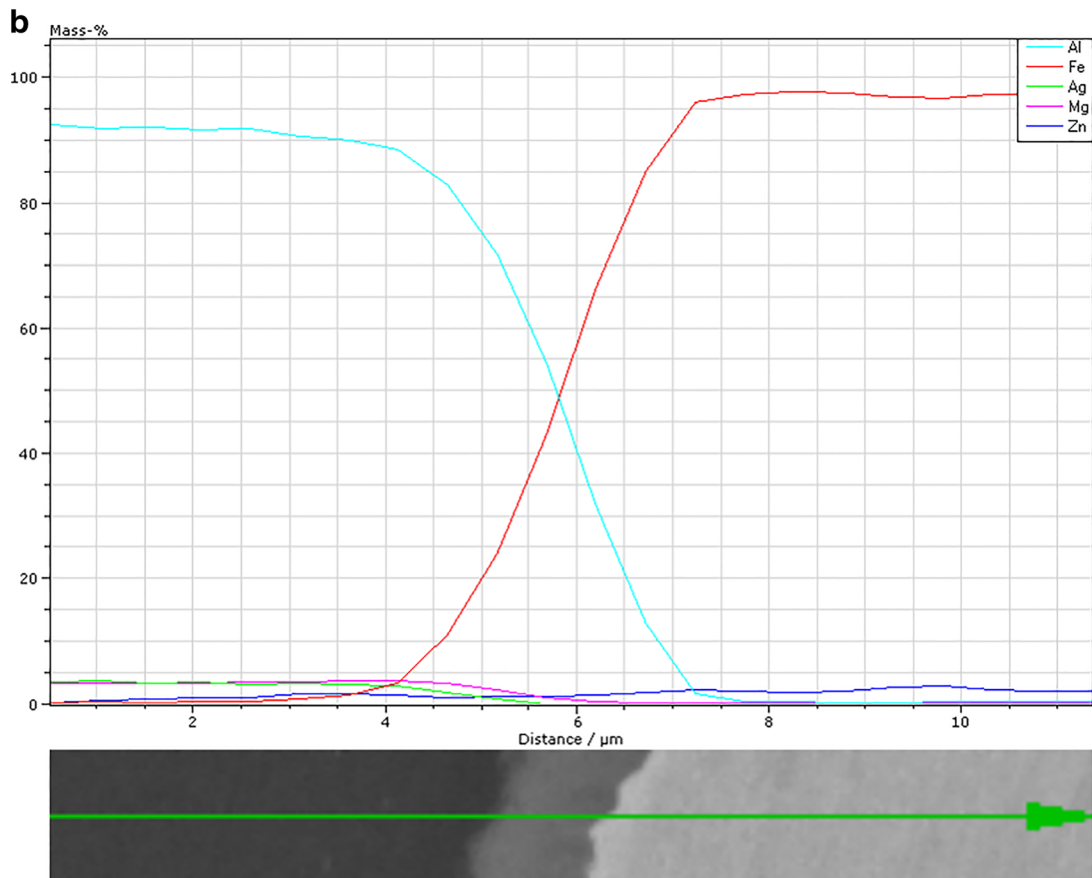
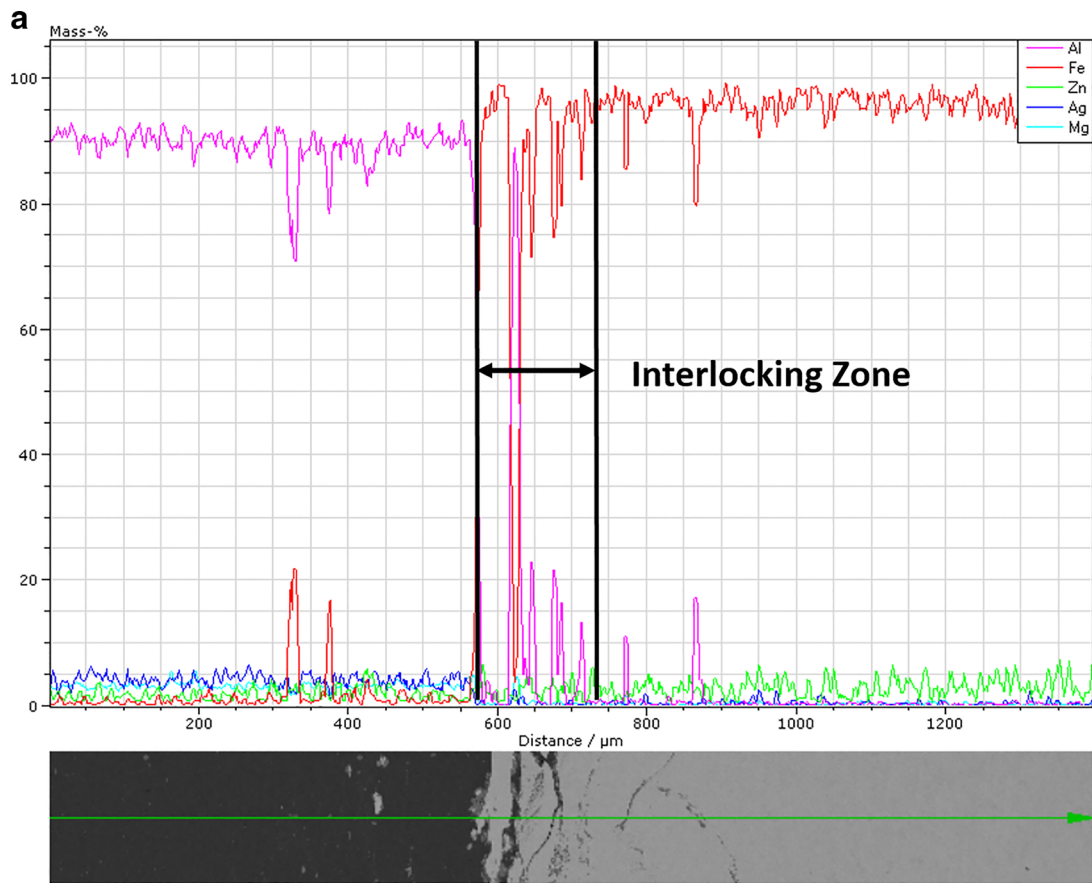
Fig. 13 Results of the tensile shear test of the FSW_{new} with different welding passes

5.4 Analysis of step 4

FSW_{new} with a single pass weld was examined further using SEM coupled with EDX analysis and microhardness testing. Haghshenas et al. [15] suggest that controlling the thickness and types of IMCs formed at the weld interface is vital to achieving a weld with optimum mechanical performance. The presence of IMCs with high aluminum content is detrimental to mechanical performance unlike those with high Fe composition. The EDX analysis along a line passing through the centerline of the weld region shows a 175- μ m-thick layered structure (interlocking zone) with an aluminum content that ranges from 10 to 23% (Fig. 14a). Higher magnification reveals a uniform IMC layer with 1- μ m thickness, which is present along the entire weld interface, having an aluminum content varying from 20 to 60% (Fig. 14b).

Figure 15 shows the EDX maps of that structure. A large amount of AA was mixed with the steel forming the IMC layers.

The AA5754-H22 is a strain hardened partially annealed material (not fully stabilized) with a microhardness of approximately 68 HV0.2. In the steel, the microhardness values of the stir zone and thermomechanically affected zone (TMAZ) are higher than of the steel base material due to strain hardening. The average microhardness value is 107 HV0.2 of the steel base material, 142 HV0.2 of the steel TMAZ, and 193 HV0.2 of the steel stir zone. Figure 16 shows the microhardness map of the weld zone. The microscopic image (magnified area) shows the point with the highest microhardness value, which is 284 HV0.2, located on the advancing side of weld zone where a considerable amount of IMCs are present. Furthermore, the distribution of the microhardness values emphasizes the influence of the original geometry of the innovative joint design, with higher values at the regions corresponding to the peaks of the wave-shaped feature than in remaining area. This is due to the formation of IMCs in these regions as a result of the extra plastic deformation.



◀ **Fig. 14** Analysis of the chemical composition along the line crossing through **a** the multiple layered structures at the center of FSW_{new}; **b** the continuous intermetallic compound (IMC) layer across the joint interface

6 Conclusions

An innovative overlap joint concept was tested, in single-pass and multipass configurations, and compared to conventional overlap welding for FSW of aluminum alloy AA5754-H22 to steel DX54. The main conclusions from the research are the following:

- The innovative overlap joint concept with two-pass welds produced the overall best mechanical properties with 50% of the UTS of the AA base material in tensile shear tests.
- The peeling test results for single pass welds showed higher resistance of the innovative overlap joint concept when compared with the conventional joint concept.
- The innovative overlap joint concept has shown better mechanical strength properties with relatively lower weld pitch ratios (rotation speed versus travel speed). At the lower weld pitch ratios, the mechanical resistance of the welds was mainly affected by the reduced residual effec-

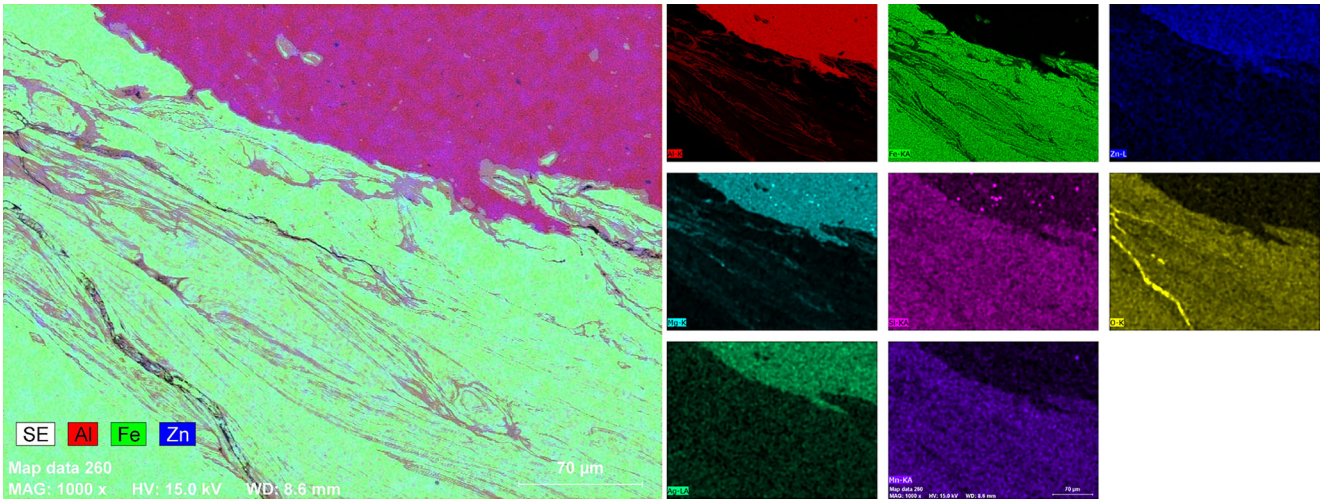
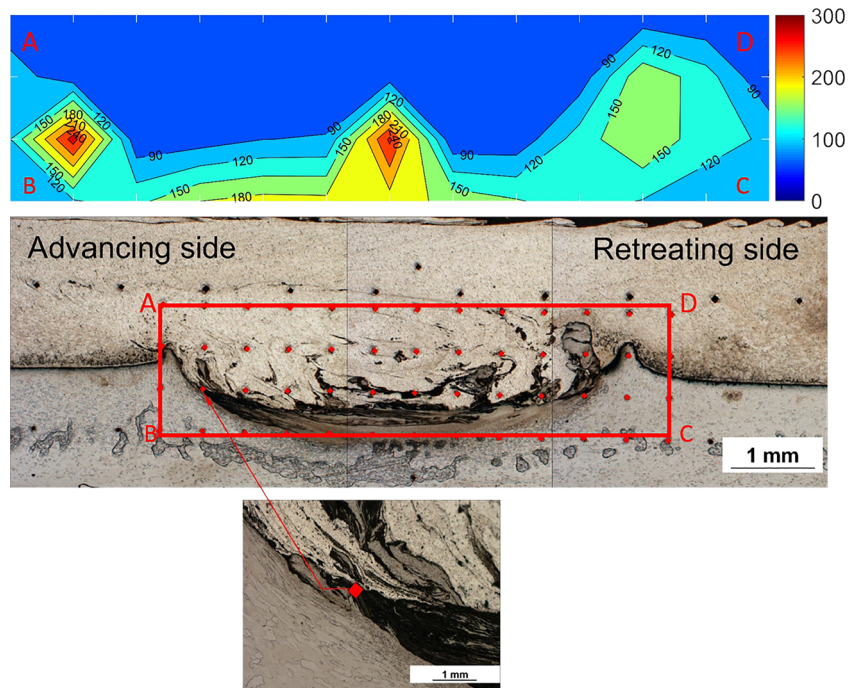


Fig. 15 EDX maps across the multiple layered structures located at the joint interface

Fig. 16 Map of the Vickers microhardness (HV0.2) on cross section of FSW_{new} single pass



tive thickness of the AA base material due to flow of the steel into the aluminum (formation of the hook imperfection), mainly at the flow side, i.e., the retreating side of the welds.

- The innovative overlap joint with one pass produced a larger hook compared to the conventional overlap joint. The larger hook reduced the effective thickness of the AA sheet which considerably influenced the mechanical resistance of the welds.
- Voids were found at the Al-Fe interface, which can be observed in the optical macrographs. The intermediate travel speed conditions presented the lowest level of void formation in terms of size and quantity. Multipass welding increased the material flow within the processing zone, which was helpful to eliminate the voids.
- The layered structure was dependent on the axial forging force. Higher axial forging force generated larger layered structures and higher internal pressure, which facilitated the consolidation of the joining. Moreover, the layered structure provided extra solid-state joining mechanisms, which increased the mechanical resistance of the welds.
- The optical micrographs showed that swirl-like patterns, and IMCs were preferentially formed at higher weld pitch ratios as a result of higher heat input.
- The two-pass joint exhibited the best mechanical properties compared with single-pass or three-pass welds, due to higher stirring efficiency with a more uniform mechanical interlocking region.
- EDX analysis showed a uniform IMC layer with thickness of 1 μm present along the entire weld interface, the aluminum content of these IMCs ranged from 20 to 60%.
- The microhardness distribution closely follows the original geometry of the innovative overlap joint.

Open Access This article is distributed under the terms of the Creative Commons Attribution 4.0 International License (<http://creativecommons.org/licenses/by/4.0/>), which permits unrestricted use, distribution, and reproduction in any medium, provided you give appropriate credit to the original author(s) and the source, provide a link to the Creative Commons license, and indicate if changes were made.

References

1. Kenevisi MS, Khoie SM (2012) A study on the effect of bonding time on the properties of Al7075 to Ti-6Al-4V diffusion bonded joint. *Mater Lett* 76:144–146
2. Lee CJ, Kim JY, Lee SK, Ko DC, Kim BM (2010) Parametric study on mechanical clinching process for joining aluminum alloy and high-strength steel sheets. *J Mech Sci Technol* 24(1):123–126
3. Figner G, Vallant R, Weinberger T, Enzinger N, Schröttner H, Pašič H (2009) Friction stir spot welds between aluminum and steel automotive sheets: influence of welding parameters on mechanical properties and microstructure weld world (2009) 53(1): R13-R23
4. Abe Y, Mori K, Kato T (2012) Joining of high strength steel and aluminium alloy sheets by mechanical clinching with dies for control of metal flow. *J Mater Process Tech* 212(4):884–889
5. Dehghani M, Amadeh A, Mousavi SA (2013) Investigations on the effects of friction stir welding parameters on intermetallic and defect formation in joining aluminum alloy to mild steel. *Mater Design* 49:433–441
6. Thomas WM, Nicholas ED (1997) Friction stir welding for the transportation industries. *Mater Design* 18(4–6):269–273
7. Leitao C, Leal RM, Rodrigues DM, Loureiro A, Vilaça P (2009) Mechanical behaviour of similar and dissimilar AA5182-H111 and AA6016-T4 thin friction stir welds. *Mater Design* 30(1):101–108
8. Kimapong K, Watanabe T (2004) Friction stir welding of aluminum alloy to steel. *Weld J* 83(10):277–282
9. Haghshenas M, Abdel-Gwad A, Omran AM, Gökçe B, Sahraeinejad S, Gerlich AP (2014) Friction stir weld assisted diffusion bonding of 5754 aluminum alloy to coated high strength steels. *Mater Design* 55:442–449
10. Uzun H, Dalle Donne C, Argagnotto A, Ghidini T, Gambaro C (2005) Friction stir welding of dissimilar Al 6013-T4 to X5CrNi18-10 stainless steel. *Mater Design* 26(1):41–46
11. Coelho RS, Kostka A, Sheikhi S, dos Santos J, Pyzalla AR (2008) Microstructure and mechanical properties of an AA6181-t4 aluminum alloy to HC340LA high strength steel friction stir overlap weld. *Adv Eng Mater* 10(10):961–972
12. Liu X, Lan S, Ni J (2014) Analysis of process parameters effects on friction stir welding of dissimilar aluminum alloy to advanced high strength steel. *Mater Design* 59(7):50–62
13. Sur Bang H, Seon Bang H, Hong Jeon G, Hyun Oh I, Seung Ro C (2012) Gas tungsten arc welding assisted hybrid friction stir welding of dissimilar materials Al6061-T6 aluminum alloy and STS304 stainless steel. *Mater Design* 37:48–55
14. Liu X, Lan S, Ni J (2015) Electrically assisted friction stir welding for joining Al 6061 to TRIP 780 steel. *J Mater Process Tech* 219: 112–123
15. Chen ZW, Yazdani S, Littlefair G (2012) Effects of tool positioning on joint interface microstructure and fracture strength of friction stir lap Al-to-steel welds. *J Mater Sci* 48(6):2624–2634
16. Kimapong K, Watanabe T (2005) Lap joint of A5083 aluminum alloy and SS400 steel by friction stir welding. *Mater Trans* 46(4): 835–841
17. Elrefaey A, Gouda M, Takahashi M, Ikeuchi K (2005) Characterization of aluminum/steel lap joint by friction stir welding. *J Mater Eng Perform* 44(1):10–17
18. Cantin GMD, David SA, Thomas WM, Lara-Curzio E, Babu SS (2005) *Sci Technol Weld Joi* 10(3):269–280